

Document downloaded from:

<http://hdl.handle.net/10251/122868>

This paper must be cited as:

Payri, R.; Bracho Leon, G.; Gimeno, J.; Bautista-Rodríguez, A. (2018). Rate of injection modelling for gasoline direct injectors. *Energy Conversion and Management*. 166:424-432. <https://doi.org/10.1016/j.enconman.2018.04.041>



The final publication is available at

<https://doi.org/10.1016/j.enconman.2018.04.041>

Copyright Elsevier

Additional Information

Rate of injection modelling for gasoline direct injectors

Raul Payri*, Gabriela Bracho, Jaime Gimeno, Abian Bautista

CMT - Motores Térmicos, Universitat Politècnica de València, Edificio 6D, 46022, Valencia, Spain.

Abstract

Awareness of climate change, fossil fuel availability, and pollutants has been growing which have pushed forward the effort in cleaner engines. In this aspect, the gasoline engines have more improving margin than diesel engines. To have a more efficient combustion, injection systems had evolved from old Port Fuel Injectors to modern Gasoline direct injections which are the used by engine manufacturers nowadays. In this study, within the framework of the Engine combustion network (ECN), the so named Spray G is modelled. This gasoline direct injector was developed by Delphi with the intention of getting a better understanding of the gasoline spray. The model is focused on the Rate of Injection (ROI) signal, whose results are presented in order to help engine calibration and modelling for an extensive range of configurations without the need for experimental measurements.

Keywords: Gasoline, ECN Spray G, rate of injection, 0-D modelling

1. Introduction

Internal combustion engines have shaped the modern world socially and economically. Since the first patented automobile, the auto market has been growing steadily to become one of the biggest industries today. However, the
5 increasing amount of engines has led to concerns about emissions. Regulations

*Corresponding author. E-mail address: rpayri@mot.upv.es

arose in order to control those, thus to be in the market engine manufacturers had to meet emission targets through engine optimization[1, 2, 3]. A good fuel-air mixture could improve combustion and efficiency which led reduced pollutants. This is mainly achieved by the fuel injection system and the injection strategy. Early injection systems for gasoline include carburetor, which provides little control on the injection. Later, Port Fuel Injection (PFI) technology led to better control in the demand of fuel [4]. At that point gasoline engines usually have been cleaner by means of toxic emissions and pollutants than diesel engines because of the combustion of a homogeneous mixture at relatively low temperature. However, the latter advantage is diminished when looking at fuel economy and CO₂ emissions. The research path to improve the performance went into new strategies that required better control of the fuel injected[5] as well as the use of common rail injection system [6]. The Gasoline Direct Injection (GDi) technology in gasoline engine was pursued to perform more refined injection strategies which have the potential to increase performance, fuel economy and performance of gasoline engines[7, 8]. For instance, some challenging scenarios that the GDi technology could improve are engine acceleration and in cold starts. Although some predictions state that GDi systems are expected to overtake PFI systems by 2020, for the moment GDi engines have several essential drawbacks such as emissions, complexity, cost etc., that prevent them from being widely accepted[4, 9].

The advancements in engine performance can be done using different analysis techniques. Combustion diagnosis models in gasoline are based in [10, 11], which measure the instantaneous pressure in the cylinder and determine the rate of heat release (RoHR). Other studies analyze the reactive spray properties such as Payri et al. [12]. Combustion diagnosis are necessary for better control equations of the thermal process in the engine [13]. Conversely, Computational Fluid Dynamic (CFD) together with engine testing allows to obtain information of the flow field and permit to estimate the trends of the emissions to act accordingly, by means of 0D, 1D and 2-3D simulations[14, 15, 16]. For the diagnostics, it

| Nomenclature | | | |
|---------------------|--|------|-----------------------------------|
| ΔP | Difference between injection and back pressure | EOE | End of Energizing |
| | | EOI | End of injection |
| \dot{m}_{exp} | Stabilized rate of injection (mass flow) | ET | Energizing time |
| | | GDi | Gasoline direct injection |
| ρ_f | Density of the fuel | Pb | Back pressure |
| R^2 | Coefficient of determination | PFI | Port Fuel Injection |
| CFD | Computational Fluid Dynamics | Pr | Rail pressure |
| | | RoHR | Rate of heat release |
| DOI | Duration of Injection | ROI | Rate of injection |
| ECN | Engine Combustion Network | SOE | Start of Energizing |
| ECU | Engine Control Unit | SOI | Start of injection |
| EDM | Electrical Discharge Machining | STP | Standard Temperature and Pressure |

has to be noted that an important input parameter is the injected mass into the system and the shape of the injection event.

The measure of Rate of injection (ROI) [17], is achieved from experimental sources, with controlled and stabilized boundary conditions. These measurements are of vital importance to validate CFD models, which can provide detailed information of the injection/combustion process as seen in [17, 18, 19]. In the case of flash boiling conditions for GDi, it is crucial to validating works such as [20, 21]. Nonetheless, the number of test points that have to be measured to achieve all the desired engine conditions could be exceptionally large. Other option to get all the desired conditions is through a model of the shape of the injection rate. This will reduce the experimental matrix and supplement with all conditions that havent been measured, providing a full database of the ROI signal.

There have been studies in the modelling of the injection system for diesel engines by modelling the dynamic behaviour [22, 23, 24]. The 1D modelling

includes all the components such as pump, injector and valves, which requires to have detailed information to understand all the process geometries and physical phenomena behind. Conversely, the 0D model is understood as a black box whose outputs are obtained by mathematical expressions without considering
55 detailed knowledge of the systems. Little work has been done using this approach, however, Payri et al. [25] presented a detailed methodology to follow where a Diesel injector was modelled, including multi-injection events. In the case of Gasoline injectors there has not been done to the best knowledge of the autors.

60 In this work, the 0D ROI model of a Delphi gasoline direct injector was performed. The results will be available in order to provide a tool to the Engine Combustion Network research group and other researchers working with GDi injectors. After this model is presented, an extension of the methodology is done for a Bosch GDi injector.

65 **2. Experimental tools and hardware**

2.1. Gdi Injector

As previously mentioned, the injector used in this work is the Spray G injector which was intentionally made for research activities of the ECN group, within the Spray G topic. The nominal conditions of the spray G are depicted
70 in Table 1.

To facilitate the CFD, a gasoline surrogate has been employed. The fuel chosen to imitate the gasoline has been iso-octane (2,2,4 trimethylpentane) for being a mono-component fuel close to gasoline in specifications as seen in [26, 27]. It has a density of 692 kg/m³ (at STP) and a kinematic viscosity of 4.8x10⁻⁴
75 Pa s (at 25°C). The injector and driver (ECU) have been manufactured by Delphi, following the specifications of the group (see Table 2).

2.2. Injection systems and test conditions

A complete common rail injection system was used to generate high pressure in the test rig used in this work, similarly to the one used in [28, 26]. The system

Table 1: ECN Spray G conditions.

| Parameter | Value | Units |
|-----------------------------|------------|-------|
| Fuel | Iso-Octane | - |
| Fuel pressure (P_{inj}) | 20 | MPa |
| Fuel temperature | 90 | °C |
| Injector temperature | 90 | °C |
| Chamber Pressure | 6 | bar |
| Chamber temperature | 300 | °C |

Table 2: Injector specifications.

| Parameter | Value | Units |
|-----------------|-------------------|-------------|
| Number of holes | 8 | - |
| Inner diameter | 165 | (μm) |
| Outlet diameter | 388 | (μm) |
| Spray shape | Circular | |
| Spray Angle | 80 | ° |
| Bend Angle | 0 | ° |
| L/D ratio | 2 | - |
| Hole shape | Straight | - |
| Manufacturing | EDM | - |
| Flow rate | 15(cc/s) @ 10 Mpa | |

80 is composed of the Delphi ECN spray G injector, a trigger generator which commands the signal to the Engine Central Unit (ECU), a rail, thermo-regulator and a high pressure pump. The high pressure pump was originally acquired to provide pressure to diesel injectors. Thus, a frequency regulator was located in the pump to achieve better control under relative low injection pressure compared to diesel however common for GDi injectors. This allows operating with
85 pressure as low as 8MPa and up to 23 MPa at a relatively constant value. The

thermo-regulator permitted to set an injector holder temperature of 90°C for all experimental test conditions using glycol as cooling fluid. The back pressure was achieved providing the cavity in the test rig with nitrogen gas, and it was varied from 1 to 10 bar. The duration of the energizing time (ET) was varied between a short pulse of 220 μ s, which is representative of pilot injections, and a long pulse of 1200 μ s which is sufficient to guarantee that the needle position is at maximum lift, so the flow is controlled by the nozzle geometry. The experiments were performed in a systematic manner, changing the ET, Injection pressure and back pressure. The measurements were done once enough time passed at each condition and the values were stabilized. The executed experimental matrix is summarized in Table 3. The Reynolds number range for the injection conditions used at the nozzle exit was from 3x10⁴ to 7x10⁴.

Table 3: Test matrix for Measurements of Spray G injector.

| Parameter | Tested Values | Units |
|---------------------------|---------------------------|--------------|
| Rail pressure (Pr) | 50/80/100/120/150/180/200 | bar |
| Back pressure (Pb) | 3/6/9/15/21 | bar |
| Energizing time | 280/300/350/680/900/1200 | μ s |
| Cycles for test condition | 50 | - |

2.3. Rate of injection test rig

The mass ejected was measured using a ROI test rig, being a long-tubed type commercial equipment. The sensor in the device can measure the time-resolved injection event. The measuring principle used is the Bosch method [19], which consists in injecting into a fuel filled measuring tube. The back pressure is provided with a cavity filled with nitrogen, which avoids back pressure oscillations. The fuel ejection produces a pressure increase inside the tube, which is proportional to the rise in fuel mass. The profile of this signal relates to the rate of injection. To avoid some uncertainties described in [17], a gravimetric balance is placed downstream whose measure serve as a reference for total mass

injected. A total of 50 sample for each test point are acquired, varying energizing
110 time (ET), injection pressure, and back pressure. The measurement error on
this device is commonly around 0.5% after proper calibration [17], being more
trustworthy for longer injections. A sketch depicting the injection rate set up
can be seen in Figure 1.

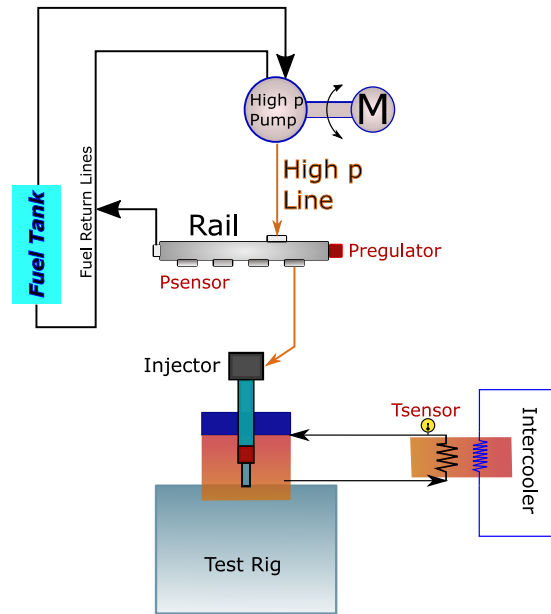


Figure 1: Sketch of the injection system.

3. Methodology

115 In this work, a simplified 0D model that imitates the ROI signal has been
developed. The model, based on mathematical expressions and correlations, is
able to reproduce the mass flow rate obtained by the experiments using the
Bosch tube method. It has to be noted that most injectors have a trapezoidal
injection rate profile, thus in certain conditions and after some tuning, the model
120 could be used for other injectors. It is focused on the injected mass and the
shape, providing some typical parameters such as ET, injection pressure, back
pressure, etc. The two primary objectives of the model are to operate at the

lowest computational cost and to produce a realistic injected mass quantity. The potential advantages of the model are that simulation results can be obtained rapidly and easily for any operating points. Moreover, it can be used in engine test bench for mass estimations as a real-time model when doing experiments or calibration activities.

The steps followed to create the model are:

- (1) To complete the mass flow rate measurements, a wide-enough test matrix established before. It should cover the operational range of the injection system (rail pressure, ET) and the pretended engine conditions that want to be reproduced by means of back pressure.
- (2) A signal decomposition is done, separating the elements that can construct the injection rate signal and at the same time selecting the most appropriate mathematical expressions that could fit such curves. Various alternatives could be considered, for instance: straight slopes, first and second order system response, polynomial, exponential and Bezier curves.
- (3) The available measured dataset is used to adjust the model expressions. For example, the coefficients are determined using the best fitting with all the measured conditions. Each equation coefficient is modelled as a function of the input parameters. This last step is an iterative process, since not always a good correlation is found at first. Depending on the ROI shape, several trials and errors are necessary, until the form of the equations and the coefficients obtained satisfies the requirements or are representative enough for all the conditions.

At the latter step, sometimes there is not a simple expression that is representative for all the conditions thus separations among rail pressures or distinction between long and short injections are necessary to find a fit of the coefficients good enough for all the conditions.

150 **4. ROI ECN Spray G modelling**

At first, the shape of the ROI signal is analysed. The curve is composed of the average of the 50 measures for each condition. It is easier to start with longer injections since they have the particularity to maintain similar shape almost independently of any injection condition. Long injections have a trapezoidal shape, whereas short injections have a more triangular-like one. The most
 155 accessible manner to address the modelling is to decompose this forms and relate then with mathematical expressions. The Figure 2 shows a standard ROI shape for this injector.

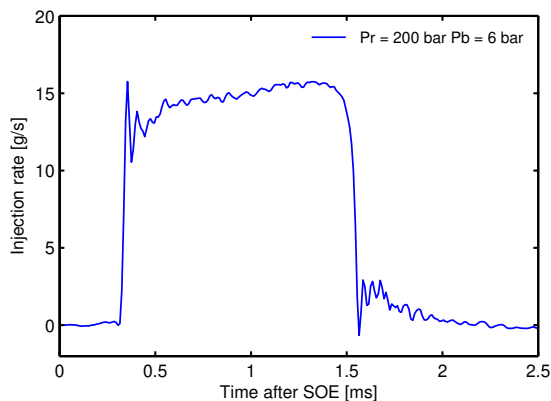


Figure 2: ROI shape.

4.1. Single injection decomposition

160 The ROI signal is separated into parametric equations in two parts: the shape function and the logistic function. The shape function is the trapezoidal silhouette which is defined by a compromise of simplest mathematical expression and best accuracy. The functions used to describe it were straight slopes for opening and closing stages and second-order Bezier curves to soften the corners
 165 (defined by Cs_x, Cs_y, Ce_x and Ce_y). Lastly, eight parameters that defined the shape are parameterized: start slope, end slope, start of injection (SOI), duration of injection (DOI) and the four control points for the Bezier curves.

The Figure 3 depicts the eight parameters. For this modelling, the overshoot at the start of the injection is not considered because the added noise to the signal is not good for CFD modelling. Besides because adding this complexity that could be over-amplified by the sensor does not compensate the added complexity in the expressions.

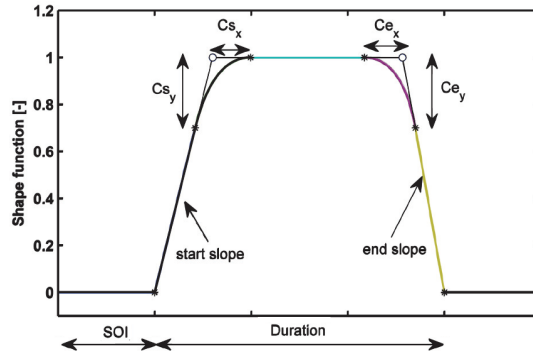


Figure 3: sketch for the shape function decomposition.

As it can be noticed, at the maximum of the signal (full needle lift) there is a slight increment at a certain point of the ROI shape. This is addressed by means of a logistic function. This function represents a step response with smoothed corners. The parameters that define the logistic functions are $X0$, AX and AY . The first one sets the point where the step starts. Then, AX and AY establish the length and height of the step, as it can be observed in Figure 4. The logistic function is depicted in equation (1). Then, the equation (2) represents the specific logistic function, where \bar{m} is the averaged mass flow rate.

$$L(t) = \frac{AY}{1 + \exp\left(\frac{-(t-X0)}{AX}\right)} \quad (1)$$

$$y = \bar{m} \cdot L(t) \quad (2)$$

The coefficients of the logistic function are adjusted to the experimental data using linear and non-linear fittings. A non-dimensional curve is obtained for doing further parameterization. It is shape function $S(t)$ (Figure 5), and

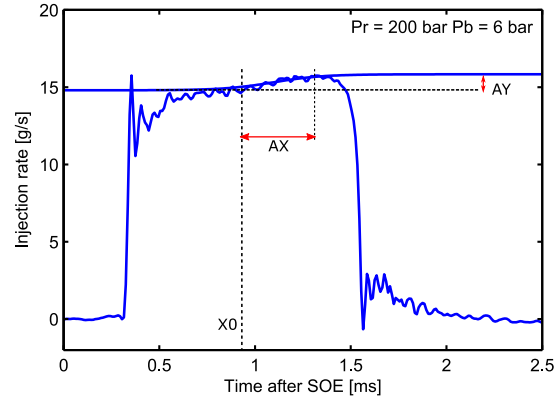


Figure 4: logistic function over the crest of a ROI signal.

185 it is obtained by dividing the real mass flow rate signal by $\dot{m} \cdot L(t)$, resulting in an easier non-dimensional curve for parameterization as it is shown in equation (3).

$$S(t) = \frac{\dot{m}(t)}{\dot{m} \cdot L(t)} \quad (3)$$

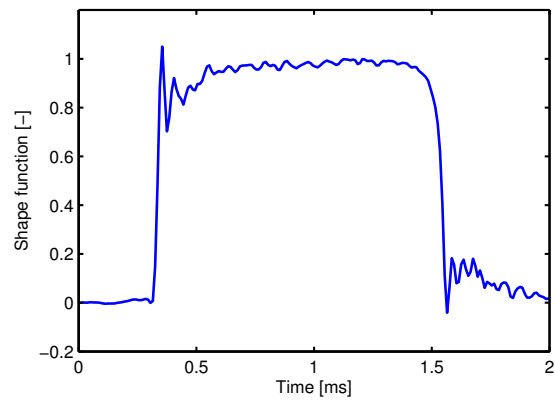


Figure 5: Shape function.

4.2. Variable dependency construction

All the extracted parameters have to be set as a function of the input parameters, which can be back pressure, rail pressure and energizing time.

190 First, the stationary mass flow is modelled. It is reached when the needle is completely lifted, such as the flow velocity is only constrained at the hole exit. This state is characterized employing Bernoulli and mass conservation equation [29].

Bernoulli's theoretical velocity (u_b) can be represented as a function of the
195 rail pressure (Pr) and back pressure (Pb) shown in equation 4. Then, this velocity is included in the expression derived from the mass conservation, which is the mass flow rate (equation 5). Where \dot{m} is the mass flow rate, ρ_f is the liquid density, A0 represents the cross-section area of all orifices and Cd is the discharge coefficient.

$$u_b = \sqrt{\frac{2(Pr - Pb)}{\rho_f}} \quad (4)$$

$$\dot{m} = Cd \cdot A0 \cdot \rho_f \cdot u_b \quad (5)$$

200 Combining these two equations the mass flow parameterization can be written as a function of the pressure drop as shown in equation 6. A0, Cd and ρ_f are represented in form of coefficients since they change little or are constant in the range of the injection conditions.

$$\dot{m} = C1 + C2\sqrt{Pr - Pb} \quad (6)$$

The coefficients C1 and C2 are adjusted to the experimental data. This is
205 achieved by linear and non-linear fittings, minimizing the relative error and the statistical number which uses the interval of the normal distribution. The fit of the experimental hydraulic characterization of the nozzle is depicted Figure 6. It can be observed that the flow rate, represented in the y-axis, increases linearly with the increase of square root of the pressure drop, represented in the
210 x-axis, which is the expected behaviour of a non-cavitating nozzle.

Next, considering the opening and closing slopes, they depend on the velocity of the needle movement. In this case, it has to be noticed that this injector is direct acting type, using a solenoid to create the magnetic field to influence the

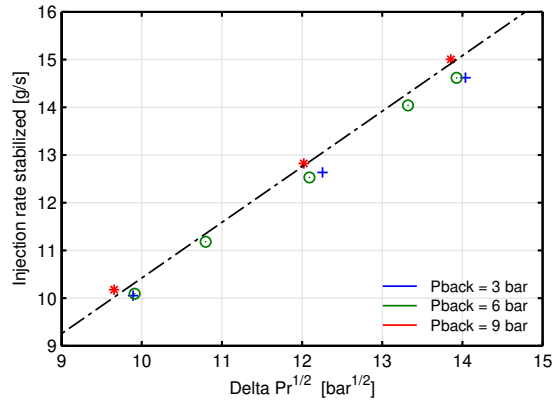


Figure 6: Mass flow against square root of pressure drop. Experimental data and fitted curve.

needle. The movement of the needle is ruled by force equilibrium between the
 215 pressure difference, effective area (where the pressure is applied) and magnetic
 field in one side, and a spring in the other side. Due to the difficulty to measure
 the magnetic field and spring force (the injector would need to be broken to ac-
 cess those parts), the opening and closing slopes are represented by the pressure
 difference between rail and back pressures, and the rest of the parameters should
 220 be included in the expression by means of fitting coefficients. The acquisition of
 the equation that represents the slopes is a challenge and as mentioned before
 is achieved by an iterative process of trial and error. After various iterations,
 equations (7) and (8) were found, which were the best polynomial expression
 that fit the opening and closing slopes respectively. The comparison of the fit-
 225 ted curves compared to the experimental data can be observed in Figure 7 and
 Figure 8. It has to be noticed that in this figures not all the experimental data
 is presented because a really loaded and hard to read figure would be instead.
 Nevertheless, the equation is adjusted using all the experimental data available.
 For this two figures, only ET of 1.2ms and injection pressures of 100 to 200 bar
 230 are displayed.

$$O = C_{O_1} + C_{O_2} \cdot Pr + C_{O_3} \cdot \sqrt{Pr} + C_{O_4} \cdot Pb + C_{O_5} \cdot Pr \cdot Pb \quad (7)$$

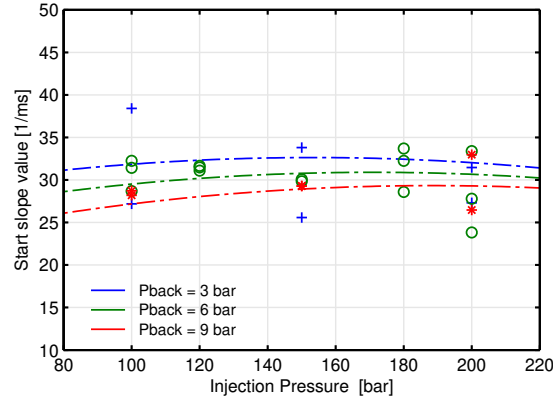


Figure 7: Experimental data and curve of Opening slopes.

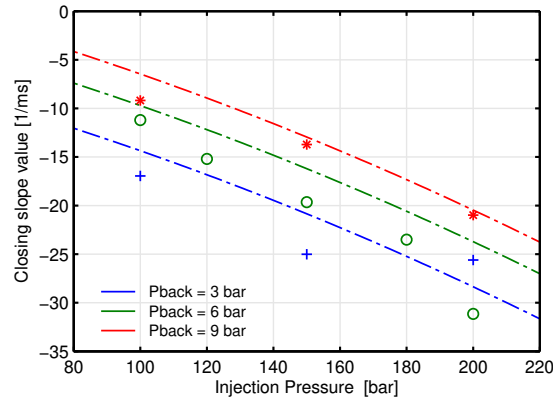


Figure 8: Experimental data and curve of closing slopes.

$$C = C_{C_1} + C_{C_2} \cdot Pr + C_{C_3} \cdot \sqrt{Pr} + C_{C_4} \cdot Pb + C_{C_5} \cdot \sqrt{Pb} \quad (8)$$

Having set the opening and closing slopes, the next step is to model the Start of Injection (SOI), which is demarcated as the time difference between the commanded signal (electric pulse) and the delay that appears in the injector. The SOI has not effect on the ROI shape, nevertheless, it sets the initial point of the curve, and it is very important for engine testers and combustion modellers. It is necessary for the injection time location in the engine map as well as CFD simulations. The main physical parameters that affects the SOI are the

235

rail pressure and the back pressure whose force components are applied on the
 needle. It could be considered the flow velocity in the interior of the sac as well,
 however this is a function of the pressure as explained before. Thus, the SOI can
 be parameterized as it is shown in equation (9). Figure 9 depicts the correlation
 for the SOI, in which experimental data using all the ETs and injection pressures
 of 100 to 200 bar are displayed. Although the tendency is hard to appreciate, it
 can be observed increased SOI for higher Pback. However, the range of variation
 of SOI value is small.

$$SOI = C_{SOI_1} + C_{SOI_2} \cdot Pr + C_{SOI_3} \cdot Pb \quad (9)$$

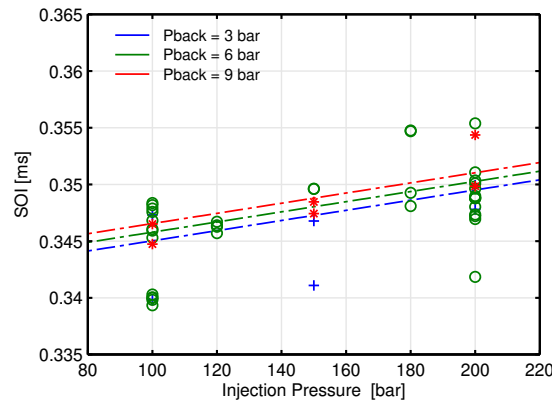


Figure 9: Fitted curve and experimental data for the SOI.

To close, the last parameter that is modelled is the end of injection (EOI).
 It depends primarily in the electrical pulse, which is the cause for the magnetic
 field and needle movement. However, it also depends on the inner volume and
 sac pressure difference and finally on the spring that pushes the needle back
 when the coil is not energized anymore. Normally, the injection duration is
 longer than the ET duration because of the inertia of the components.

To isolate the event, the EOI was modelled establishing the SOI as the origin
 in time, so the hydraulic delay is not included. The dependant variables were
 Pb, Pr and End of Energizing (EOE). It can be expected that for small ET, the

255 needle could not be totally lifted so when the electrical pulse ends, the time to
return to the closing position is shorter. On the contrary, when the ET is large,
the needle reaches its maximum position and when the pulse ends, it will close
slower than in the other case. The Figure 10 depicts this behaviour. Internal
geometric characteristics impact on the EOI, however they were included in the
260 modelled coefficients in equation 10, which is the result of the best fit found.

$$EOI = C_{EOI_1} + C_{EOI_2} \cdot Pb + C_{EOI_3}/Pr + C_{EOI_4} \cdot EOE + C_{EOI_5}/Pr^2 \quad (10)$$

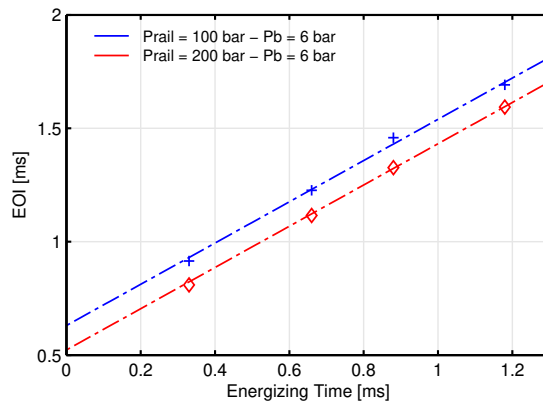


Figure 10: Fitted curve and experimental of end of injection.

All the acquired equations and fittings performed were intent to achieve a coefficient of determination (R^2) close to one. It was obtained at least an R^2 of 0.88, which would confirm that observed data is replicated by the model.

4.3. Validation

265 When the model expressions are acquired with sufficiently low deviation, a
final step of validation of the model is performed. Two main comparisons are
used as a tool to validate the model. The comparison is made with several
experimental measurements including two injection pressure and various ET.
The first comparison is shown in both Figure 11 and Figure 12, in which it can
270 be seen both rate of injection signals for the model and the experiments. It has

been chosen as injection pressure 100 bar and 200 bar since are representative for high and low injection pressures for this kind of injector. It can be observed that the model qualitatively captures the shape of the ROI signal. It can be appreciated that the opening and closing slopes are well reproduced. The SOI is well capture too, however, the EOI is little deviated for Prail of 200 bar and the second shortest ET. Moreover, although there is some deviation in the upper right corner of the trapezoid shape, it does affect little the total mass injected.

On the other hand, Figure 13 depicts the total mass injected (integral of the ROI shape) versus energizing time, both for the model and the experimental measurements. It can be seen that exists little deviation between the model and experimental and the maximum differences found are lower than 8% for reasonable short injections, when the shape of the ROI signal changes and there is not stabilized region (the flow rate is not dominated by the nozzle discharge coefficient [18, 22]).

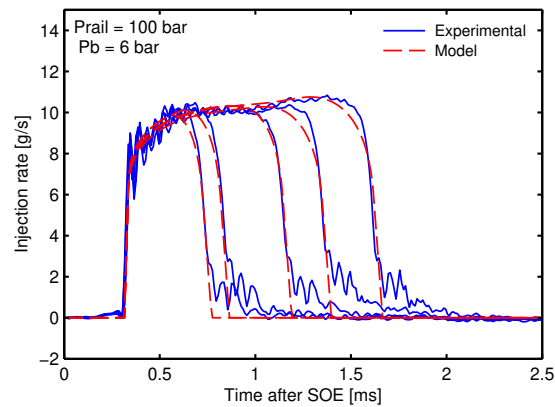


Figure 11: Experimental and modelled rate of injection signal for 100bar.

The measurements performed for a representative range of conditions have resulted in a very well characterized injector. Although the model captures well enough the injector behaviour, it has to be noticed that it has its limitations since the coefficients chosen are not universal. Its implementation outside the measured ranges or injector type should be executed carefully.

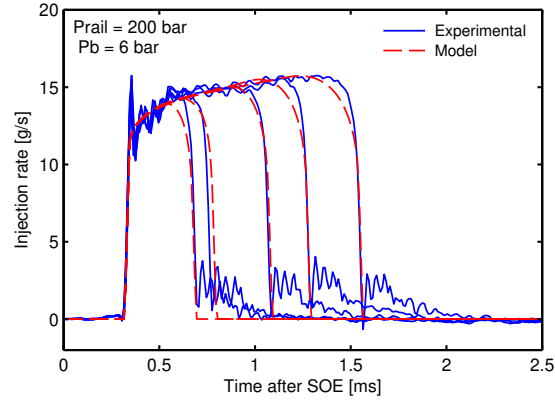


Figure 12: Experimental and modelled rate of injection signal for 200bar.

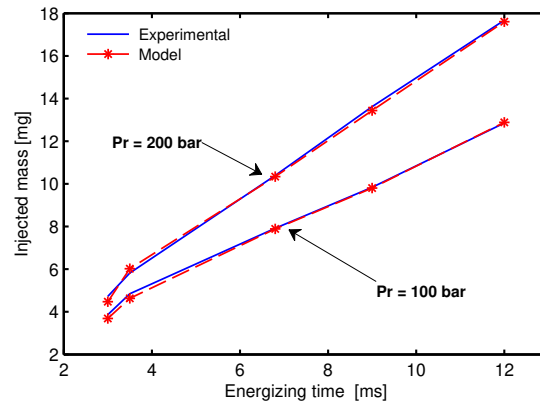


Figure 13: Experimental and modelled injected mass for 100 and 200 bar.

290 5. Extension to other gasoline injectors

To broaden the application of the model, ROI measurements of other solenoid type gasoline injector were performed. Fewer data were available for the new injector as shown in Table 4. Even though there were not measurements of the new injector available for the same ET, the ROI signal shape is relatively similar
 295 to the one of the ECN spray G, as it can be appreciated in Figure 14. There is some difference in the opening event: some overshoot occurs in the Delphi injector, whereas the other presents it mildly. The main discrepancy of this injector manufactured by Bosch is that the orifice diameter is greater than the Spray

G injector and it has a different number of them, so the model should include
 300 these parameters as an input to overcome the discrepancy. Characteristics of
 the second injector are shown in Table 5.

Table 4: Available measured data of the Bosch injector.

| Parameter | Tested Values | Units |
|---------------------------|--------------------|---------|
| Rail pressure (Pr) | 100/150/200 | bar |
| Back pressure (Pb) | 10 | bar |
| Energizing time | 500/1000/1500/2000 | μs |
| Cycles for test condition | 50 | - |

Table 5: Injector specifications.

| Parameter | Value |
|-----------------|-----------------|
| Number of holes | 6 |
| Inner diameter | 205 (μm) |
| Spray shape | Circular |
| Hole shape | Straight |

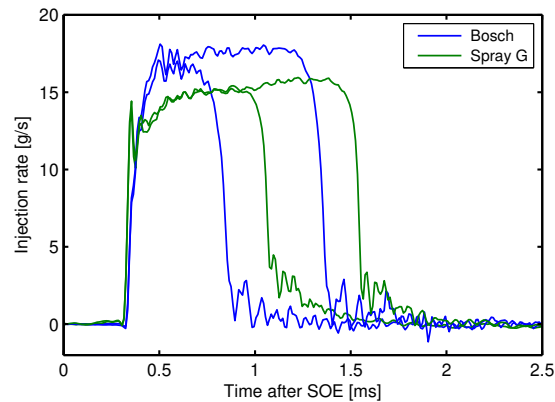


Figure 14: ROI shape for the two injectors.

5.1. Adjustment based on geometry

As seen before both injectors have similar signal shape, however, for the same injector pressure the stabilized value achieved for the Bosch injector is higher. This is due to considerable bigger orifices of the injector, so to adapt the model, the stationary mass flow has to be obtained regarding the outlet area of the injector. To allow this flexibility in the model, the equation derived to obtain the level of stabilized mass flow (eq. 6), has to be modified to include the characteristic geometry in the equation, which is present in eq 5. Rearranging the expression (eq. 11), the new model should implement a new C1 that would fit for all injectors. Where At is the cross-section area of all orifices.

$$\dot{m} = C1 \cdot At \cdot \left(1 + \frac{C2}{C1} \sqrt{Pr - Pb}\right) \quad (11)$$

Linear and non-linear fittings are applied minimizing the relative error to find the coefficient. The results of this fittings are presented in Figure 15. The flow rate increases linearly with the square root of the pressure drop, which is the case of these injectors and a requirement for the application of the model as stated before.

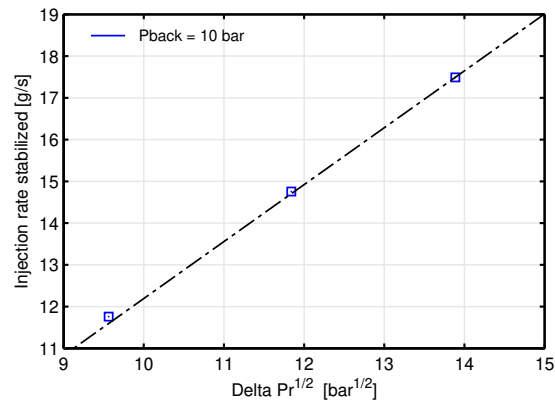


Figure 15: Stabilized injection rate for the Bosch injector, model in the black line and experimental in the blue points.

5.2. Validation

This final step is done similarly to the case of the first injector. To validate the model comparisons of the ROI signal shape and total injected mass flow are performed against the model. The first comparison is done by depicting the ROI shape, as it can be seen in Figure 16 and Figure 17. Qualitatively, it can be appreciated that the model captures relatively well the shape of the experimental signal. However, it lacks reproducing the opening and closing slopes mostly for the case of 200 bar and the top left corner of the trapezoid shape for all cases. Moreover, although the end of injection is not as well reproduced as for the Spray G injector the model is acceptable to reproduce the signal property.

The second comparison is shown in Figure 18, by plotting the modelled and experimental injected mass. The bigger differences are found in the shorter injections, where the signal starts to change from a trapezoid shape with a stabilized region to a shorter triangle shape typical of pilot injections [10] [12]. Although this part is where the model has difficulties, the differences in all the operating points represented are below 5%.

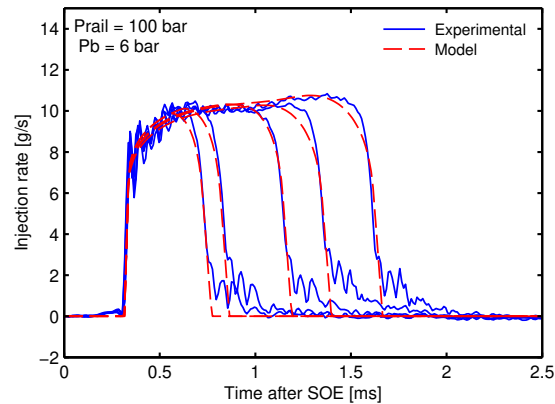


Figure 16: Experimental and modelled rate of injection signal for 100bar for the Bosch injector.

Albeit the VIM does not model the internal dynamics of the injector, its application to this Bosch injector demonstrates that it could be applied to an injector with similar characteristics as long as the total outlet area is known and the nozzle represents a similar flow pattern.

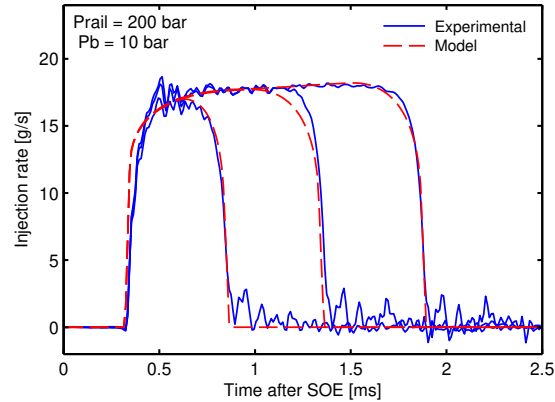


Figure 17: Experimental and modelled rate of injection signal for 200bar for the Bosch injector.

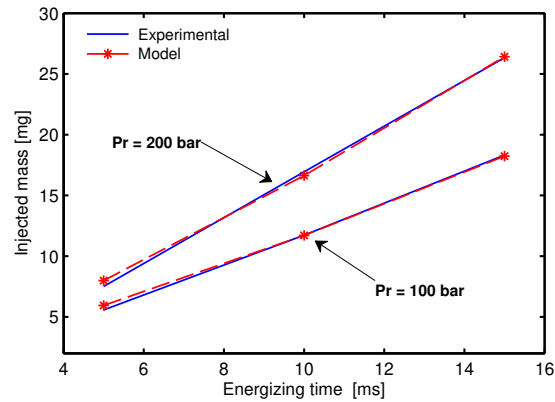


Figure 18: Experimental and modelled injected mass for 100 and 200 bar for the Bosch injector.

6. Conclusions

This work has presented a model of the Rate of injection for the ECN spray G, which is a solenoid driven Gasoline direct acting injector, and how it could be adapted to similar injectors. It was constructed from a set of experimental data measured at CMT, which provided a well characterized injector. The model is built using correlations and complex equations which takes into account ET, mass, durations and rail and chamber pressure as inputs to assemble the final ROI signal. Nevertheless, injection pressure is the parameter that has the most

345 influence in the output signal in terms of total mass and shape. The physical
phenomena were considered to help approximating the expressions to what was
happening during the injection event. One important limitation of the model
is that the simulations outside the measured range should be used carefully,
since the empirical coefficients are chosen for the measured range. Another
350 limitation is the use of the model for pilot injections, since it was difficult to
obtain reliable ROI measurements with low variability, and its modelling was
therefore a challenge with strongly non-linear behaviour. The extension of the
model for the Bosch injector functioned reasonably good, being the latest a very
similar injector type, which its major difference is the outlet section area of the
355 orifices. The limitations of the extended model are the same as the Spray G
model besides the careful application of it in the case of cocked injectors for
instance. Finally, the model presented a total mass difference error below 5%
in most of the cases, which can be considered good accuracy since is on the
range of the natural error of the injector. The 0D model of the ECN spray G
360 would be available for spray and combustion simulations which will streamline
the process of understanding the injection phenomena.

Acknowledgements

This article was supported by Generalitat Valenciana through AICO/2018
under the project *Nuevos conceptos en inyección de gasolina (NCIG)* and through
365 *Ayudas de la Conselleria de Educació, Cultura y esports para la promoció y di-*
namizaci3n de parques científcos (PPC/2018. DOCV del 07/11/2017). Further-
more, the authors would like to express their gratitude to the collaboration of
the lab technicians Jose Enrique and Omar. Finally, Maria Martinez and Daniel
Vaquerizo for assistance and help.

370 References

- [1] J. Benañes, R. Novella, D. De Lima, P. Tribotté, Analysis of combustion concepts in a newly designed two-stroke high-speed direct injection

- compression ignition engine, *International Journal of Engine Research* 16 (2015) 52–67.
- 375 [2] T. V. Johnson, Vehicular Emissions in Review, *SAE International Journal of Engines* 5 (2012) 2012–01–0368.
- [3] C. F. Powell, A. L. Kastengren, Z. Liu, K. Fezzaa, The Effects of Diesel Injector Needle Motion on Spray Structure, *Journal of Engineering for Gas Turbines and Power* 133 (2010) 12802.
- 380 [4] H. Zhao, *Advanced direct injection combustion engine technologies and development*, Woodhead Publishing Limited, Cambridge, 2010.
- [5] D. J. Duke, A. L. Kastengren, K. E. Matusik, A. B. Swantek, C. F. Powell, R. Payri, D. Vaquerizo, L. Itani, G. Bruneaux, R. O. Grover, S. Parrish, L. Markle, D. Schmidt, J. Manin, S. A. Skeen, L. M. Pickett, Internal and near nozzle measurements of Engine Combustion Network Spray G gasoline direct injectors, *Experimental Thermal and Fluid Science* 88 (2017) 608–621.
- 385 [6] D. Han, K. Li, Y. Duan, H. Lin, Z. Huang, Numerical study on fuel physical effects on the split injection processes on a common rail injection system, *Energy Conversion and Management* 134 (2017) 47–58.
- 390 [7] L. Marchitto, D. Hampai, S. Dabagov, L. Allocca, S. Alfuso, C. Polese, A. Liedl, GDI spray structure analysis by polycapillary X-ray u-tomography, *International Journal of Multiphase Flow* 70 (2015) 15–21.
- [8] E. A. Rivera, N. Mastro, J. Zizelman, J. Kirwan, R. Ooyama, Development of Injector for the Direct Injection Homogeneous Market using Design for Six Sigma, *SAE Technical Paper* 2010-01-0594 (2010).
- 395 [9] C. Wang, H. Xu, J. M. Herreros, J. Wang, R. Cracknell, Impact of fuel and injection system on particle emissions from a GDI engine, *Applied Energy* 132 (2014) 178–191.

- 400 [10] G. Hoffmann, B. Befrui, A. Berndorfer, W. F. Piock, D. L. Varble, Fuel System Pressure Increase for Enhanced Performance of GDi Multi-Hole Injection Systems, *SAE International Journal of Engines* 7 (2014) 2014–01–1209.
- [11] A. C. Alkidas, Combustion advancements in gasoline engines, *Energy Conversion and Management* 48 (2007) 2751–2761.
- 405 [12] R. Payri, F. J. Salvador, J. Gimeno, J. E. Peraza, Experimental study of the injection conditions influence over n-dodecane and diesel sprays with two ECN single-hole nozzles. Part II: Reactive atmosphere, *Energy Conversion and Management* 126 (2016) 1157–1167.
- [13] Z. Yuan, J. Liu, J. Fu, Q. Liu, S. Wang, Y. Xia, Quantitative analysis on the thermodynamics processes of gasoline engine and correction of the control equations for heat-work conversion efficiency, *Energy Conversion and Management* 132 (2017) 388–399.
- 410 [14] D. Jarrahbashi, S. Kim, B. W. Knox, C. L. Genzale, Computational analysis of end-of-injection transients and combustion recession, *International Journal of Engine Research* 18 (2017) 1088–1110.
- [15] N. Atef, J. Badra, M. Jaasim, H. G. Im, S. M. Sarathy, Numerical investigation of injector geometry effects on fuel stratification in a GCI engine, *Fuel* 214 (2018) 580–589.
- 420 [16] C. Mohapatra, G. Jacobsohn, E. Baldwin, D. Schmidt, Modeling sealing in transient injector simulations, in: American Society of Mechanical Engineers, Fluids Engineering Division (Publication) FEDSM, volume 1A-2017, 2017. doi:10.1115/FEDSM2017-69309.
- [17] R. Payri, F. J. Salvador, J. Gimeno, G. Bracho, A new methodology for correcting the signal cumulative phenomenon on injection rate measurements, *Experimental Techniques* 32 (2008) 46–49.
- 425

- [18] M. Coppo, C. Dongiovanni, Experimental Validation of a Common-Rail Injector Model in the Whole Operation Field, *Journal of Engineering for Gas Turbines and Power* 129 (2007) 596.
- 430 [19] W. Bosch, The Fuel Rate Indicator: A New Measuring Instrument for Display of the Characteristics of Individual Injection, SAE Technical Paper 660749 (1966).
- [20] E. T. Baldwin, R. O. Grover, S. E. Parrish, D. J. Duke, K. E. Matusik, C. F. Powell, A. L. Kastengren, D. P. Schmidt, String flash-boiling in gasoline
435 direct injection simulations with transient needle motion, *International Journal of Multiphase Flow* 87 (2016) 90–101.
- [21] H. Guo, H. Ding, Y. Li, X. Ma, Z. Wang, H. Xu, J. Wang, Comparison of spray collapses at elevated ambient pressure and flash boiling conditions using multi-hole gasoline direct injector, *Fuel* 199 (2017) 125–134.
- 440 [22] N.-H. Chung, B.-G. Oh, M.-H. Sunwoo, Modelling and injection rate estimation of common-rail injectors for direct-injection diesel engines, *Proceedings of the Institution of Mechanical Engineers, Part D: Journal of Automobile Engineering* 222 (2008) 1089–1001.
- [23] R. Payri, B. Tormos, F. J. Salvador, A. H. Plazas, Using one-dimensional
445 modelling codes to analyse the influence of diesel nozzle geometry on injection rate characteristics, *International Journal of Vehicle Design* 38 (2005) 58–78.
- [24] A. E. Catania, A. Ferrari, M. Manno, E. Spessa, Thermal Effect Simulation in High-Pressure Injection System Transient Flows, SAE Technical Paper
450 2004-01-0532 (2004).
- [25] R. Payri, J. Gimeno, R. Novella, G. Bracho, On the rate of injection modeling applied to direct injection compression ignition engines, *International Journal of Engine Research* (2016).

Raul Payri, Gabriela Bracho, Jaime Gimeno, Abian Bautista; Rate of injection modelling for gasoline direct injectors; *Energy Conversion and Management*, vol. 166, no. February, pp. 424432, 2018.

- 455 [26] R. Payri, J. Gimeno, P. Martí-Aldaraví, D. Vaquerizo, Internal flow characterization on an ECN GDi injector, *Atomization and Sprays* 26 (2016) 889–919.
- [27] S. Jonnalagedda, T. Nguyen, B. Zhou, A. Sobiesiak, Numerical investigation of HCCI combustion in an IDI type diesel engine fueled with isooctane, *SAE Technical Papers* (2011).
- 460 [28] R. Payri, J. Gimeno, P. Martí-Aldaraví, D. Vaquerizo, Momentum Flux Measurements on an ECN GDi Injector, in: *SAE Technical Paper 2015-01-1893*, 2015. URL: <http://papers.sae.org/2015-01-1893/>. doi:10.4271/2015-01-1893.
- 465 [29] R. Payri, F. J. Salvador, J. Gimeno, A. Garcia, Flow regime effects over non-cavitating Diesel injection nozzles, *Journal of Automobile Engineering* 226 (2011) 133–144.